Journal of Crystal Growth 507 (2019) 389–394

Contents lists available at ScienceDirect

Journal of Crystal Growth

journal homepage: www.elsevier.com/locate/jcrysgro

Structural characteristics of m-plane AlN substrates and homoepitaxial films

Milena Bobea Graziano[a,b,*], Isaac Bryan[b], Zachary Bryan[b], Ronny Kirste[b], James Tweedie[b], Ramon Collazo[b], Zlatko Sitar[b]

[a] Oak Ridge Associated Universities Postdoctoral Fellowship, Sensors and Electron Devices Directorate, Army Research Laboratory, Adelphi, MD 20783, United States
[b] Department of Materials Science and Engineering, North Carolina State University, Raleigh, NC 27695, United States

ARTICLE INFO

Communicated by M.S. Goorsky

Keywords:
A1. Characterization
A1. High resolution x-ray diffraction
A1. Surface structure
A1. Crystal structure
A3. Metalorganic chemical vapor deposition
B1. Nitrides

ABSTRACT

Homoepitaxial non-polar AlN films were realized on m-plane $(10\bar{1}0)$-oriented AlN single crystals by metalorganic chemical vapor deposition (MOCVD). The microstructural properties of m-plane AlN substrates and homoepitaxial films were assessed by means of atomic force microscopy and high resolution x-ray diffraction characterization. Results indicated that both m-plane AlN substrates and films possessed exceptional structural quality, with some anisotropic mosaic distributions due to the quasi-bulk nature of the non-polar single crystals. An increase in the MOCVD growth temperature was noted to minimize the degree of inherited mosaic anisotropy without altering the m-plane AlN film growth rate, indicating that high temperature growth is critical to produce optimal film crystallinity. A dramatic change in the film surface morphology from heavily faceted "slate-like" features to monolayer steps was observed as the growth temperature was increased. The "slate-like" surface morphology produced low intensity cross-streaks in symmetric $(10\bar{1}0)$ reciprocal space maps, tilted about 18° away from the $(10\bar{1}0)$ crystal truncation rod. The orientation of these diffuse streaks corresponds to the physical alignment of the slates with respect to the substrate surface normal. X-ray line scans and defect-selective reciprocal space mapping confirmed that these low intensity streaks are solely dependent on this peculiar surface structure produced at low MOCVD growth temperatures and unrelated to basal plane stacking faults or other extended defects. All observations confirm that high quality III-nitride epitaxial structures on m-plane AlN substrates are attainable with controllable MOCVD growth processes, as demanded for future high performing AlN-based non-polar devices.

1. Introduction

High-performing, non-polar III-nitride-based optoelectronic devices are currently pursued as part of a strong global initiative towards highly efficient next-generation solid-state lightning technologies. The use of $(11\bar{2}0)$, a-plane, or $(10\bar{1}0)$, m-plane, growth surfaces for heteroepitaxial quantum well structures has proven to be advantageous, as it can eliminate the inherent large spontaneous and piezoelectric polarization fields known to hinder radiative recombination rates in the polar (0001), c-plane-oriented light-emitting devices [1,2]. In the last decade, promising results in GaN-based non-polar systems have suggested the potential to achieve high-brightness light-emitting diodes (LEDs) and laser diodes (LDs) with enhanced radiative carrier recombination, lack of wavelength shift (no quantum-confined Stark effect), and increased internal quantum efficiency [3–10]. These remarkable advances correspond to exceptional improvements in the crystalline and optical quality of non-polar epitaxial structures due to the increased availability and use of non-polar GaN bulk crystals as substrate materials. Unfortunately, GaN substrates are not suitable for the growth of high-Al AlGaN-based structures, as required to develop optoelectronics that can operate in the deep ultraviolet (DUV) spectral region [11–15]. As such, the development of DUV devices with theoretically predicted efficiencies and remarkable overall performance may demand the use of non-polar AlN single crystals for the growth of high quality non-polar AlN and high Al-content AlGaN materials.

Recently, non-polar $(10\bar{1}0)$ m-plane-oriented AlN wafers cut and processed from AlN single crystal boules grown by physical vapor transport (PVT) have become available [16–18]. Efforts towards the development of m-plane AlN homoepitaxy led to the first reported successful growth of m-plane AlN homoepitaxial thin films by metalorganic chemical vapor deposition (MOCVD) [19,20]. As in non-polar m-plane GaN homoepitaxy, a strong dependence of the AlN film surface

* Corresponding author at: Oak Ridge Associated Universities Postdoctoral Fellowship, Sensors and Electron Devices Directorate, Army Research Laboratory, Adelphi, MD 20783, United States.
E-mail address: milena.b.graziano.ctr@mail.mil (M. Bobea Graziano).

https://doi.org/10.1016/j.jcrysgro.2018.07.012
Received 22 January 2018; Received in revised form 8 June 2018; Accepted 12 July 2018
Available online 14 December 2018
0022-0248/

morphology to the MOCVD growth temperature has been evidenced and explained by changes in surface energetics and adatom diffusion lengths [19,21]. Similarly, the optical characteristics of m-plane AlN homoepitaxial films have been discussed, where a high oxygen impurity incorporation has been noted at low MOCVD growth temperatures due to preferential incorporation into $(000\bar{1})$ faceted slates [20]. Regarding the crystallinity of m-plane AlN PVT-grown substrates and MOCVD-grown homoepitaxial films, most studies report x-ray rocking curves (XRCs) as a measure of microstructural quality [19,22]. However, extensive reports on their crystallographic features are yet to be published. In this study, we report on the particular structural characteristics of these non-polar III-nitride materials and investigate the occurrence of notorious issues, including film strain, crystallographic anisotropy, and population of basal plane stacking faults (BPSFs) and/or other extended defects.

2. Experimental details

The m-plane AlN substrates were sliced and processed from AlN single crystalline boules grown in the $[000\bar{1}]$ by PVT [16,18,23,24]. Prior to epitaxy, substrates were treated using a procedure published elsewhere [17]. Homoepitaxial m-plane AlN films were deposited using a vertical cold-walled MOCVD reactor at temperatures between 1150 °C (high supersaturation) and 1550 °C (low supersaturation) under a total reactor pressure of 20 Torr and V/III ratio of 1000. The surface morphology and crystalline properties of all m-plane AlN substrates and homoepitaxial films were investigated using an Asylum Research MFP-3D atomic force microscope (AFM) in tapping mode and a PANalytical X'Pert MRD system (Cu Kα1, λ = 1.54056 Å), respectively. XRCs (ω-scans), 2θ-ω line scans, and reciprocal space maps (RSMs) were employed to assess the crystalline quality of the substrates and grown homoepitaxial films. The double-axis configuration was set for XRCs, utilizing a four-bounce Ge (2 2 0) monochromator on the incident beam and an open detector. For 2θ-ω radial scans and RSMs, a triple-axis configuration was used, where an additional three-bounce Ge analyzer crystal was placed before the detector in order to achieve a higher resolution. X-ray incident beam orientation with respect to the in-plane sample alignment (surface azimuth angle) was monitored for all measurements in order to distinguish dependences of diffraction features on crystallographic orientation and identify the presence and magnitude of structural anisotropy in both m-plane AlN substrates and films.

3. Results and discussion

Fig. 1 shows the characteristic topography of an as-received m-plane PVT-AlN substrate. AFM imaging resolved atomic steps of 2.7 Å height, corresponding to one m-plane monolayer. For all substrates, an average root mean square (RMS) roughness of less than 100 pm was identified, along with no pits, scratches, or other deleterious polishing-induced defects.

Like semi-polar oriented crystals, non-polar III-nitrides possess unit cells with lower in-plane rotational symmetry [25]. As such, the intrinsic anisotropy of non-polar materials must be taken into account when examining the presence of crystallographic defects. The crystal quality of non-polar III-nitrides may be identified with traditional XRC analysis, but it demands several measurements taken along the sample azimuth to identify directional dependences for mosaic broadening [25–30]. Following this method, symmetric $(10\bar{1}0)$ XRCs were recorded for m-plane AlN substrates at several azimuth angles, where the largest variation in the XRC width was identified for measurements taken with the diffraction plane aligned parallel and perpendicular to $[000\bar{1}]$ (Fig. 2). For XRCs recorded parallel to the $[000\bar{1}]$, the XRC line shapes were sharp and narrow, having full-width at half maximum (FWHM) values below 30 arc sec, within the resolution limit of the XRD system in the double-axis configuration and lower than previously reported

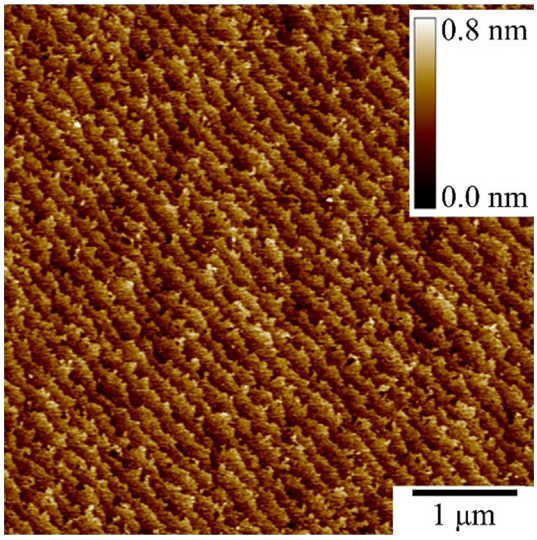

Fig. 1. $5 \times 5\,\mu m^2$ AFM scan of m-plane AlN substrate surface free of polishing damage. The image shows monolayer steps of 2.7 Å step height (one m-plane monolayer) and RMS roughness of below 100 ppm.

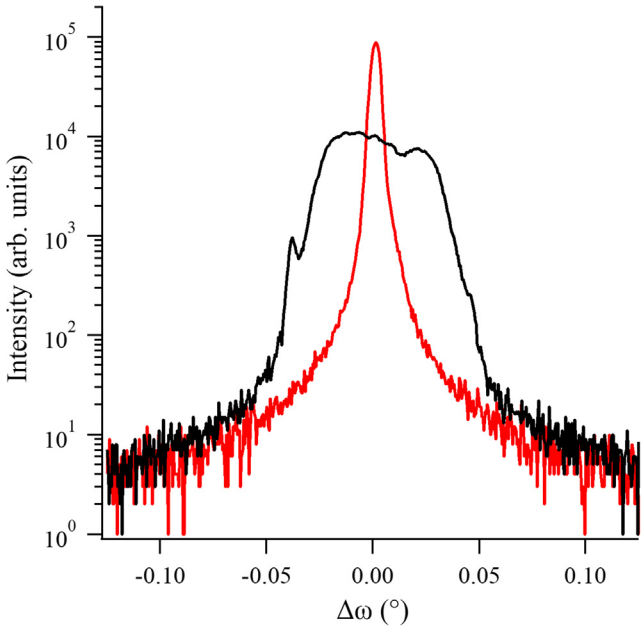

Fig. 2. Characteristic symmetric $(10\bar{1}0)$ XRCs of m-plane AlN substrates, taken parallel (red) and perpendicular (black) to $[000\bar{1}]$. (For interpretation of the references to colour in this figure legend, the reader is referred to the web version of this article.)

values on PVT-grown m-plane AlN substrates with very low dislocation densities [16]. For XRCs measured perpendicular to the $[000\bar{1}]$, the XRCs exhibited broad, multi-peaked line shapes and FWHMs ranging from 136 to 158 arc sec. Because these substrates are sliced from PVT-grown, (0001)-oriented AlN crystal boules, the variation in XRC broadening is not a strain-induced effect. Instead, the significant variation with azimuth angle is attributed to the original mosaic tilt and twist of the c-oriented AlN crystal boule from which the m-plane AlN substrates are sliced and prepared. This observation, often denoted as the "quasi-bulk" nature of the non-polar substrate, has also been reported by Chichibu et al. [31] and Kagaya et al. [32] for XRCs measured for free-standing m-plane GaN substrates harvested from $[000\bar{1}]$-oriented boules.

Homoepitaxial films were deposited onto a set of m-plane AlN substrates with comparable crystal quality and a common surface

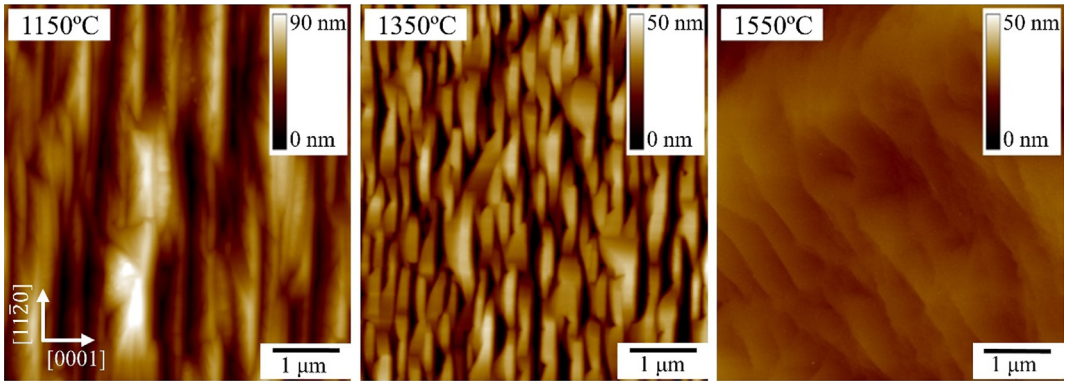

Fig. 3. 5 × 5 μm^2 AFM images of (10$\bar{1}$0) homoepitaxial AlN films grown at three different temperatures. The images reveal a dramatic decrease in film surface roughness as the film growth temperature is increased.

misorientation of 0.45° of [10$\bar{1}$0] towards [0001]. The growth temperature was varied from 1150 °C to 1550 °C, while all other growth parameters were kept identical. Within the investigated temperature range, two characteristic film surface morphologies were identified, shown in Fig. 3. For m-plane AlN films grown at and below 1350 °C, a preferential faceting of "slate-like" surface features was observed. The features were oriented in the [0001], elongated along a direction that appeared slightly misoriented from the [11$\bar{2}$0]. Above 1350 °C, atomically smooth surfaces were obtained with no preferential faceting and RMS roughness values as low as 0.4 nm, as shown for the 1550 °C film. At these higher growth temperatures, monolayer steps were resolved with step-heights identical to those seen on the m-plane AlN substrates (Fig. 1).

For all films, the symmetric (10$\bar{1}$0)rocking curves measured with the diffraction plane parallel to the [0001] exhibited very narrow peaks, ranging between 13 and 28 arc sec (Fig. 4a). Interestingly, all films exhibited a reduction in the XRC broadening anisotropy with sample orientation when compared to the m-plane AlN substrate, becoming almost negligible for films grown above at and above 1350 °C (Fig. 4b). Among the films, this temperature-dependent effect in the XRC width may correspond to differences in the lateral coherence length of the films, which can be correlated to the AFM images (Fig. 3) [33]. However, the lack of large (10$\bar{1}$0)XRC broadening anisotropy in the homoepitaxial films in contrast to the substrate is possibly explained by the expansion of highly-oriented bulk crystal grains with increasing temperature, while other slightly misoriented grains become suppressed. Subsequent homoepitaxial film deposition results in highly-oriented film domains, narrowing the (10$\bar{1}$0) XRC. This temperature-dependent effect in the XRC width may correspond to differences in the lateral coherence length of the films, which can be correlated to the AFM images (Fig. 3) [33]. More importantly, these differences are unrelated to changes in the film growth rate, as triple-axis 2θ-ω radial scans centered at the (10$\bar{1}$0) reflection resolved Pendellösung fringes that confirmed a film thickness of about 1.2 μm for all deposition temperatures [20]. This effect is also not a consequence of complex film-substrate relationships, as there are no differences in lattice and thermal expansion coefficients that could induce high densities of dislocations and stacking faults that would manifest XRC width changes. The measurements confirm that m-plane AlN homoepitaxy proceeded without the generation of crystallographic defects that would lead to an increase of the film mosaic tilt. Furthermore, as skew-symmetric (20$\bar{1}$1) curves for all films ranged in FWHM values between 20 and 26 arc sec, there were no detectable contributions to mosaic twist, either.

Accurate values for non-polar III-nitride lattice constants may be obtained by examining a series of reflections, but is often complicated by the required scanning geometries and large variations in diffracted intensity [25]. For this reason, several 2θ-ω line scans were recorded for a set of nine skew-symmetric reflections [34]. The absolute Bragg

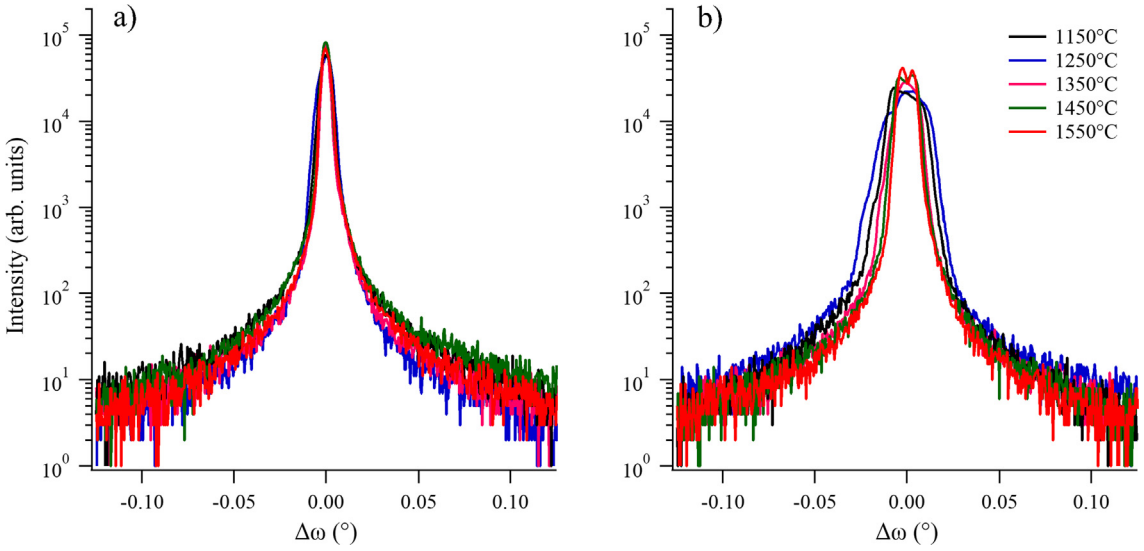

Fig. 4. Symmetric (10$\bar{1}$0) XRCs taken **a)** parallel and **b)** perpendicular to [0001] for m-plane AlN homoepitaxial films grown at different temperatures. All films exhibit a dramatically reduced mosaic anisotropy than that observed for the m-plane AlN bulk substrates (Fig. 2). Negligible variations correspond to films grown at and above 1350 °C.

Table 1
Experimental values for *a* and *c* lattice parameters for m-plane AlN homoepitaxial films and PVT-grown m-plane substrate.

Sample	a (Å)	c (Å)
1150 °C	3.111 ± 0.00005	4.981 ± 0.00041
1350 °C	3.111 ± 0.00007	4.981 ± 0.00037
1550 °C	3.111 ± 0.00008	4.981 ± 0.00059
m-plane AlN substrate	3.111 ± 0.00007	4.981 ± 0.00038

angles were extracted using the pseudo-Voigt peak fitting function. The *a* and *c* lattice constants were found by means of the *d*-spacing equation for the hexagonal crystal structure. A precision of $\sim 10^{-5}$ was achieved for lattice parameters by following methodical system calibration and sample alignment, along with proper error propagation by means of weighing methods described in detail elsewhere [35]. Table 1 shows the absolute lattice parameter values for the homoepitaxial films along with those of a single crystal substrate. These results evidence that within the growth temperatures investigated for the m-plane AlN homoepitaxy, the resulting films were strain free, exhibiting lattice constant values similar to those of the substrate. This observation was also confirmed by low temperature near band edge PL characterization, where the visible Γ_1 (6.032 eV) and Γ_5 (6.040 eV) free exciton transitions also indicated that the films were strain free [20,36].

Defect-sensitive characterization by HRXRD RSMs was employed on all films to address the potential role of BPSFs on the observed surface morphology in m-plane AlN homoepitaxial layers. Unlike line scans in the reciprocal space, RSMs around multiple reflections can provide comprehensive information on crystallographic defects in epitaxial films, since a map can access the full profile of the reciprocal lattice points (RLPs). The presence of BPSFs in m-plane III-nitride films can be determined by evaluating specific diffraction features in symmetric $(h0\bar{h}0)$ RSMs [29,33,37–39]. Among the several types of stacking faults that can form in the wurtzite structure, the most commonly observed are the intrinsic I_1 and I_2-type BPSFs with I_1-type known to have the lowest formation energy and usually making up around 90% of the observed BPSFs in the non-polar III-nitrides [40]. If such defects are present in the m-plane AlN homoepitaxial films, diffuse scatter streaks along Q_x are observed in the symmetric $(h0\bar{h}0)$ RSMs. However, these are only visible when the diffraction plane is parallel to [0001] of the film, since the scattering vector in the reciprocal space must be perpendicular to the stacking faults [29,38].

Taking into account the x-ray probing direction and the stacking fault displacement vector **R**, diffraction from I_1 $\left(R = \frac{1}{6}\langle 20\bar{2}3\rangle\right)$ and I_2-type $\left(R = \frac{1}{3}\langle 1\bar{1}00\rangle\right)$ in symmetric $(h0\bar{h}0)$ RSMs will be observed according to the diffraction invisibility criterion, $g \cdot R = n$, where $\boldsymbol{g}$ is the reflection and n is any integer, zero included [29,37,39]. Therefore, BPSF diffraction is observed only around $(10\bar{1}0)$ and $(20\bar{2}0)$ reflections. By means of this analysis, maps around symmetric $(h0\bar{h}0)$ AlN reciprocal lattice points were investigated and compared.

Fig. 5 shows the $(10\bar{1}0)$ RSMs taken parallel to [0001] for m-plane AlN films grown at 1150 °C, 1350 °C, and 1550 °C. For all films, the AlN $(10\bar{1}0)$ RLPs display comparable intensity and width, in agreement with the $(10\bar{1}0)$ Bragg peak broadening measured in double-crystal XRCs (Fig. 4). These strong reflections produced an intense artifact streak that is normally only seen in bulk crystalline material, evidence for the high structural quality of the m-plane AlN homoepitaxial films [25,41]. However, the recorded maps exhibit differences in the pole diffuse scatter and the crystal truncation rod (CTR). The highest pole diffuse scatter magnitude and shortest CTR length corresponded to the 1150 °C film, which possessed a much rougher surface (Fig. 3). As the film growth temperature was increased, a decrease in the magnitude of the pole diffuse scatter and an increase in the CTR length were identified, along with a reduced intensity of diffuse cross streaks, oriented 18° away from the CTR. The cross streaks, resolved only in the lower temperature films, corresponded to facet truncation rods arising from the "slate-like" surface features. For m-plane AlN films grown above 1350 °C, the cross streaks were no longer observed in the $(10\bar{1}0)$ RSMs, as the films possessed featureless, atomically smooth surfaces. For the 1550 °C film, the RSM shows minimal pole diffuse scatter and an intense CTR, extended in length by more than $1x10^{-3}$ reciprocal lattice units (RLUs). These results were representative of the structural improvement of the m-plane AlN film surface with increasing growth temperature, an observation that can be directly correlated to the AFM images.

Fig. 6 shows the $(20\bar{2}0)$ and $(30\bar{3}0)$ RSMs taken parallel to [0001]. The

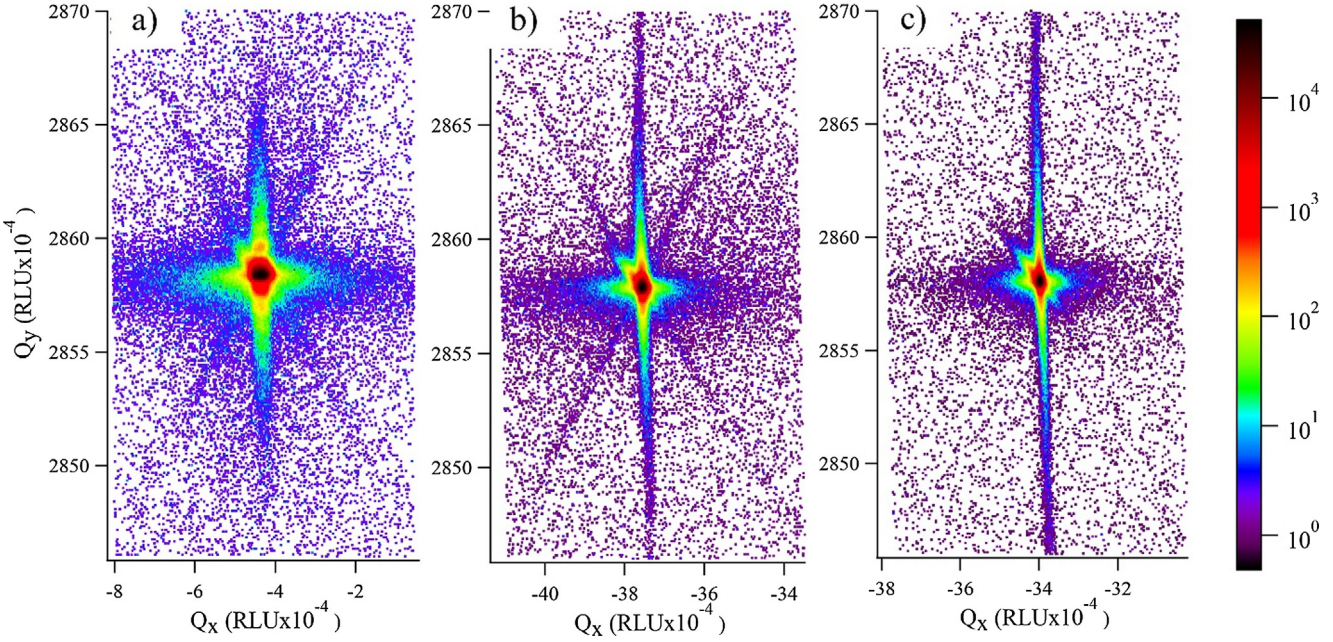

Fig. 5. RSMs of the $(10\bar{1}0)$ reflection for (a) 1150 °C, (b) 1350 °C, and (c) 1550° C. A reduction in the pole diffuse scatter and CTR length extension is observed for higher temperature films but no BPSF-related streaks are observed.

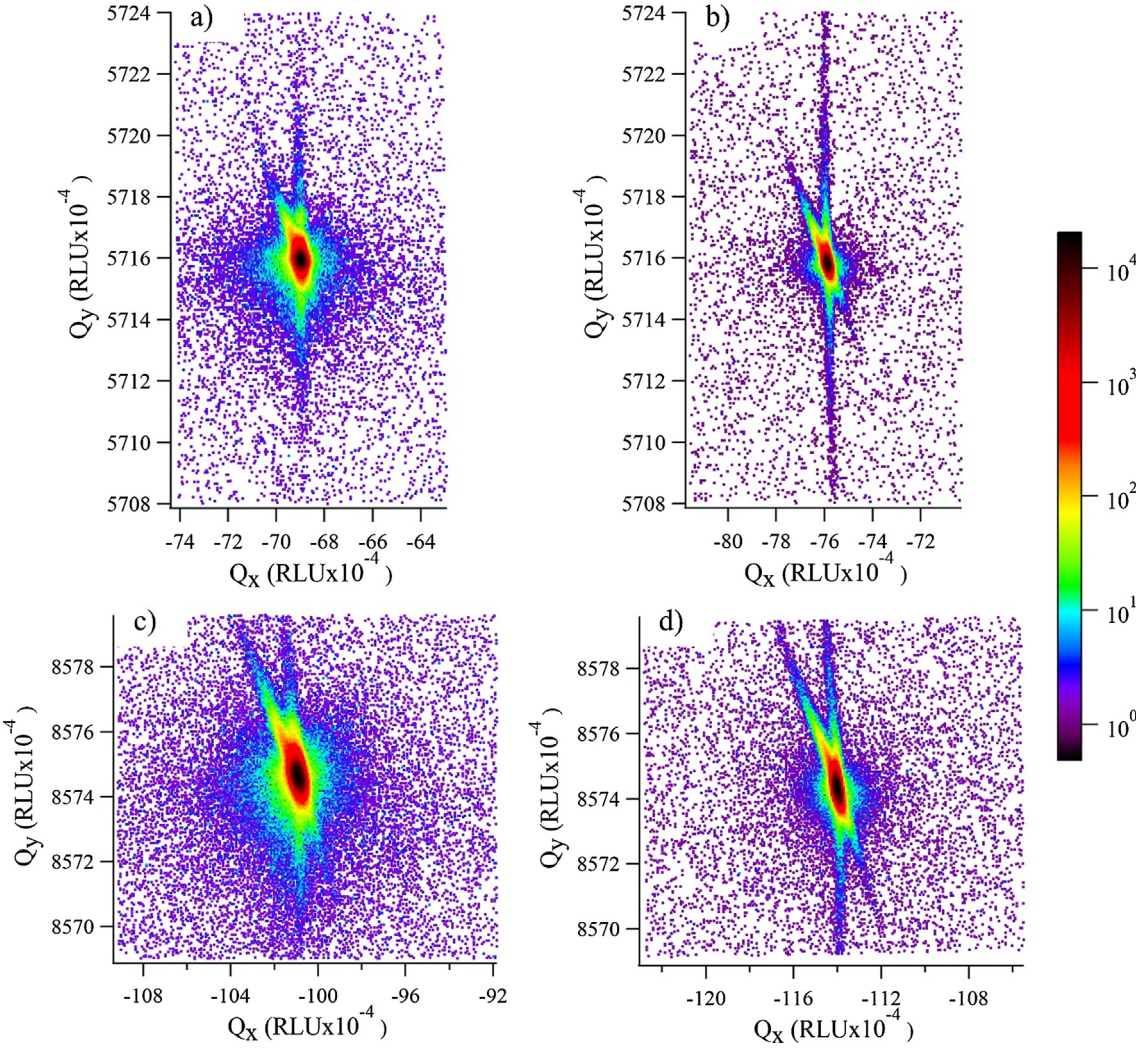

Fig. 6. Symmetric ($h0\bar{h}0$) RSMs for (a), 9c) 1150 °C and (b), (d) 1550 °C m-plane AlN films. Both the ($20\bar{2}0$) (a and b) and ($30\bar{3}0$) (c and d) reflections show a trend in the pole diffuse scatter reduction, but not satisfying the diffraction visibility criteria for BPSFs. CTR visibility is improved in the higher temperature films.

higher angle symmetric reflections also present a radial reduction of the pole diffuse scatter and elongation of the CTR as the film growth temperature was increased. Unlike non-polar a-plane GaN films studied by Moram et al. [29,38], no particular Q_x streaking was observed in any of the ($10\bar{1}0$) or ($20\bar{2}0$) maps. Since there is no characteristic diffuse streak observed in the ($10\bar{1}0$) and ($20\bar{2}0$) maps as compared to the ($30\bar{3}0$) map, the pole diffuse scatter observed in any of the m-plane AlN homoepitaxial films does not correspond to either I_1 nor I_2-type BPSFs.

It is important to note that the detection of BPSFs using this technique was employed in films that possessed BPSF density of around $10^5\,cm^{-1}$ [29,38]. The density of BPSFs was determined from plan-view transmission electron microscopy imaging and calculated from the total length of stacking faults per unit area [29,38,39]. In double-axis configuration, scans for non-polar heteroepitaxial films with known BPSF density exhibited an absolute diffuse scatter intensity of more than 300 counts per second (cps) between ($20\bar{2}0$) and ($30\bar{3}0$) curves, corresponding to an order of magnitude difference in the BPSF intensity [38]. However, for m-plane AlN homoepitaxial films, double-axis XRCs exhibited differences in diffuse scatter magnitude away from the ($20\bar{2}0$) and ($30\bar{3}0$) AlN Bragg peak that varied by less than 30 cps. Therefore, it is possible that the assessment of BPSF density by RSM diffuse scatter requires film microstructure with a certain minimum density of BPSFs, which these m-plane AlN homoepitaxial films do not seem to possess. All ($h0\bar{h}0$) RSMs confirmed that the films were either stacking-fault free or possessed a stacking fault density undetectable by HRXRD. This is an important result that confirms the achievable material quality that the homoepitaxial processes on native m-plane AlN substrates can yield.

The results presented demonstrate that the observed surface morphology in m-plane films grown at low MOCVD growth temperature is not related to in-plane film strain, dislocations, or high densities of BPSFs. The observed surface morphology was a widespread phenomenon over the entire film, an otherwise localized effect if it was determined by crystallographic defects. The resulting surface morphology in such low dislocation density substrates is determined by surface kinetics (i.e., the relationship between the terrace width and surface diffusion length), which is determined by substrate miscut and growth process supersaturation [19,21,42,43]. Thus, for m-plane AlN homoepitaxial films, the surface roughening is a controllable phenomenon that can be fully mitigated by choosing proper MOCVD growth parameters and substrate surface properties.

4. Conclusions

Structural parameters and surface features of PVT-grown m-plane AlN substrates and MOCVD-grown m-plane AlN homoepitaxial films have been investigated. Within the evaluated range of growth parameters, high quality films were achieved with significantly reduced mosaic tilt anisotropy and no biaxial film strain. Low temperature

growth (high supersaturation) resulted in rougher film surfaces that exhibited striated, “slate-like” morphology while high temperature growth produced smooth surfaces with no characteristic features. Defect-sensitive symmetric ($h0\bar{h}0$) RSMs did not reveal detectable densities of BPSFs or other extended defects that could be responsible for the resulting morphology, regardless of process parameters. Conclusively, it is the role of surface kinetics that determines the resulting film surface morphology, which can be controlled by process supersaturation. These results confirm the potential of achieving high-quality non-polar III-nitride devices on native m-plane AlN single crystalline substrates.

Acknowledgements

Partial financial support from NSF (ECCS-1508854, ECCS-1610992, ECCS-1653383), ARO (W911NF-15-2-0068, W911NF-16-C-0101), AFOSR (FA9550-14-1-0264, FA9550-17-1-0225), DARPA (W911QX-10-C-0027), and ARPA-E(DE-AR0000299) is greatly appreciated. All AlN wafers used for homoepitaxial growth were supplied by HexaTech, Inc., Morrisville, NC.

References

[1] V. Fiorentini, F. Bernardini, F.D. Sala, A. Di Carlo, P. Lugli, Effects of macroscopic polarization in III-V Nitride multiple quantum wells, Phys. Rev. B 60 (1999) 8849, https://doi.org/10.1103/PhysRevB.60.8849.
[2] P. Waltereit, O. Brandt, A. Trampert, H.T. Grahn, J. Menniger, M. Ramsteiner, M. Reiche, K.H. Ploog, Nitride semiconductors free of electrostatic fields for efficient white light-emitting diodes, Nature 406 (2000) 865, https://doi.org/10.1038/35022529.
[3] A. Chakraborty, B.A. Haskell, S. Keller, J.S. Speck, S.P. Denbaars, S. Nakamura, U.K. Mishra, Demonstration of nonpolar M-Plane InGaN/GaN light-emitting diodes on free-standing M-Plane GaN substrates, Jpn. J. Appl. Phys. 44 (2005) L173, https://doi.org/10.1143/JJAP.44.L173.
[4] K. Okamoto, H. Ohta, D. Nakagawa, M. Sonobe, J. Ichihara, H. Takasu, Dislocation-free M-Plane InGaN/GaN light-emitting diodes on M-plane GaN single crystals, Jpn. J. Appl. Phys. 45 (2006) L1197, https://doi.org/10.1143/JJAP.45.L1197.
[5] K. Iso, H. Yamada, H. Hirasawa, N. Fellows, M. Saito, K. Fujito, S.P. DenBaars, J.S. Speck, S. Nakamura, High brightness blue InGaN/GaN light emitting diode on nonpolar M-plane bulk GaN substrate, Jpn. J. Appl. Phys. 46 (2007) L960, https://doi.org/10.1143/JJAP.46.L960.
[6] M.C. Schmidt, K.-C. Kim, H. Sato, N. Fellows, H. Masui, S. Nakamura, S.P. DenBaars, J.S. Speck, High power and high external efficiency M-plane InGaN light emitting diodes, Jpn. J. Appl. Phys. 46 (2007) L126, https://doi.org/10.1143/JJAP.46.L126.
[7] M.C. Schmidt, K.-C. Kim, R.M. Farrell, D.F. Feezell, D.A. Cohen, M. Saito, K. Fujito, J.S. Speck, S.P. DenBaars, S. Nakamura, Demonstration of nonpolar M-Plane InGaN/GaN laser diodes, Jpn. J. Appl. Phys. 46 (2007) L190, https://doi.org/10.1143/JJAP.46.L190.
[8] C. Wetzel, M. Zhu, J. Senawiratne, T. Detchprohm, P.D. Persans, L. Liu, E.A. Preble, D. Hanser, Light-emitting diode development on polar and non-polar GaN substrates, J. Cryst. Growth 310 (2008) 3987, https://doi.org/10.1016/j.jcrysgro.2008.06.028.
[9] T. Detchprohm, M. Zhu, Y. Li1, Y. Xia, C. Wetzel, E.A. Preble, L. Liu, T. Paskova, D. Hanser, Green light emitting diodes on A-plane GaN bulk substrates, Appl. Phys. Lett 92 (241109) (2008), https://doi.org/10.1063/1.2945664.
[10] S.P. DenBaars, D. Feezell, K. Kelchner, S. Pimputkar, C.-C. Pan, C.-C. Yen, S. Tanaka, Y. Zhao, N. Pfaff, R. Farrell, M. Iza, S. Keller, U. Mishra, J.S. Speck, S. Nakamura, Development of gallium-nitride-based light-emitting diodes (LEDs) and laser diodes for energy-efficient lighting and displays, Acta Mater. 61 (2013) 945, https://doi.org/10.1016/j.actamat.2012.10.042.
[11] A. Khan, K. Balakrishnan, T. Katona, Ultraviolet light-emitting diodes based on group three nitrides, Nature Photon. 2 (2008) 77, https://doi.org/10.1038/nphoton.2007.293.
[12] T. Wunderer, C.L. Chua, Z. Yang, J.E. Northrup, N.M. Johnson, M. Kneissl, G.A. Garrett, H. Shen, M. Wraback, Pseudomorphically grown ultraviolet C photopumped lasers on bulk AlN substrates, Appl. Phys. Lett. 4 (2011) 092101, , https://doi.org/10.1143/APEX.4.092101.
[13] J. Xie, S. Mita, Z. Bryan, W. Guo, L. Hussey, B. Moody, R. Schlesser, R. Kirste, M. Gerhold, R. Collazo, Z. Sitar, Lasing and longitudinal cavity modes in photo-pumped deep ultraviolet AlGaN heterostructures, Appl. Phys. Lett. 102 (2013) 171102, , https://doi.org/10.1063/1.4803689.
[14] H. Hirayama, N. Maeda1, S. Fujikawa, S. Toyoda, N. Kamata, Recent progress and future prospects of AlGaN-based high-efficiency deep-ultraviolet light-emitting diodes, Jpn. J. Appl. Phys. 53 (100209) (2014), https://doi.org/10.7567/JJAP.53.100209.
[15] M. Kneissl, A brief review of III-nitride UV emitter technologies and their applications, in: M. Kneissl, J. Rass (Eds.), III-Nitride Ultraviolet Emitters: Technology and Applications, 2016, ISBN: 978-3-319-24098-5.
[16] P. Lu, R. Collazo, R.F. Dalmau, G. Durkaya, N. Dietz, B. Raghothamachar, M. Dudley, Z. Sitar, Seeded growth of AlN bulk crystals in M- and C-orientation, J. Cryst. Growth 312 (2009) 58, https://doi.org/10.1016/j.jcrysgro.2009.10.008.
[17] I. Bryan, C.-R. Akouala, J. Tweedie, Z. Bryan, A. Rice, R. Kirste, R. Collazo, Z. Sitar, Surface preparation of non-polar single-crystalline AlN substrates, Phys. Status Solidi C 11 (2014) 454, https://doi.org/10.1002/pssc.201300401.
[18] HexaTech, Inc., AlN Substrate Products < http://www.hexatechinc.com/aln-wafer-sales.html > , 2017.
[19] I. Bryan, Z. Bryan, M. Bobea, L. Hussey, R. Kirste, R. Collazo, Z. Sitar, Homoepitaxial AlN thin films deposited on M-Plane (1100) AlN substrates by metalorganic chemical vapor deposition, J. Appl. Phys. 116 (2014) 133517, , https://doi.org/10.1063/1.4897233.
[20] Z. Bryan, I. Bryan, M. Bobea, L. Hussey, R. Kirste, Z. Sitar, R. Collazo, Exciton transitions and oxygen as a donor in M-Plane AlN homoepitaxial films, J. Appl. Phys. 115 (2014) 133503, , https://doi.org/10.1063/1.4870284.
[21] J. Nishinaka, Y. Taniyasu, T. Akasaka, K. Kumakura, Surface morphology control of nonpolar M-Plane AlN homoepitaxial layers by flow-rate modulation epitaxy, Phys. Status Solidi B 254 (2017) 1600545, https://doi.org/10.1002/pssb.201600545.
[22] A. Majkić, U. Puc, A. Franke, R. Kirste, R. Collazo, Z. Sitar, M. Zgonik, Optical properties of aluminum nitride single crystals in the THz region, Opt. Mater. Express 5 (2015) 2106, https://doi.org/10.1364/OME.5.002106.
[23] D. Ehrentraut, Z. Sitar, Advances in bulk crystal growth of AlN and GaN, MRS Bull. 34 (2009) 259, https://doi.org/10.1557/mrs2009.76.
[24] Z. Herro, D. Zhuang, R. Schlesser, Z. Sitar, Growth of AlN single crystalline boules, J. Crys. Growth 312 (2010) 2519, https://doi.org/10.1016/j.jcrysgro.2010.04.005.
[25] M.A. Moram, M.E. Vickers, X-ray diffraction of III-nitrides, Rep. Prog. Phys. 72 (2009) 036502, , https://doi.org/10.1088/0034-4885/72/3/036502.
[26] T. Paskova, V. Darakchieva, P.P. Paskov, J. Birch, E. Valcheva, P.O.A. Persson, B. Arnaudov, S. Tungasmitta, B. Monemar, Properties of nonpolar A-plane GaN films grown by HVPE with AlN buffers, J. Cryst. Growth 281 (2005) 55, https://doi.org/10.1016/j.jcrysgro.2005.03.013.
[27] T. Paskova, R. Kroeger, S. Figge, D. Hommel, High-quality bulk A-plane GaN sliced from boules in comparison to heteroepitaxially grown thick films on R-Plane sapphire, Appl. Phys. Lett. 89 (2006) 051914, , https://doi.org/10.1063/1.2236901.
[28] C. Roder, S. Einfeldt, S. Figge, T. Paskova, D. Hommel, Stress and wafer bending of A-plane GaN layers on R-Plane sapphire substrates, J. Appl. Phys. 100 (2006) 103511, , https://doi.org/10.1063/1.2386940.
[29] M.A. Moram, C.F. Johnston, J.L. Hollander, M.J. Kappers, C.J. Humphreys, Understanding X-ray diffraction of nonpolar gallium nitride films, J. Appl. Phys. 105 (2009) 113501, , https://doi.org/10.1063/1.3129307.
[30] Y.G. Seo, S.H. Shin, D.S. Kim, H.D. Yoon, S.M. Hwang, K.H. Baik, Structural anisotropy and optical properties of nonpolar A-plane GaN epitaxial layers, J. Nanosci. Nanotechnol. 15 (2015) 7787, https://doi.org/10.1166/jnn.2015.11188.
[31] S.F. Chichibu, H. Yamaguchi, L. Zhao, M. Kubota, K. Okamoto, H. Ohta, Optical properties of nearly stacking-fault-free mm-Plane GaN homoepitaxial films grown by metal organic vapor phase epitaxy on low defect density freestanding GaN substrates, Appl. Phys. Lett. 92 (2008) 091912, , https://doi.org/10.1063/1.2842387.
[32] M. Kagaya, P. Corfdir, J.-D. Ganiere, B. Deveaud-Pledran, N. Grandjean, S.F. Chichibu, Implementation of spatio-time-resolved cathodoluminescence spectroscopy for studying local carrier dynamics in a low dislocation density M-Plane $In_{0.50}Ga_{0.95}N$ epilayer grown on a freestanding GaN substrate, Jpn. J. Appl. Phys. 50 (2011) 111002, , https://doi.org/10.1143/JJAP.50.111002.
[33] M.A. Moram, C.F. Johnston, M.J. Kappers, C.J. Humphreys, The effects of film surface roughness on X-ray diffraction of nonpolar gallium nitride films, J. Phys. D: Appl. Phys. 42 (2009) 135407, , https://doi.org/10.1088/0022-3727/42/13/135407.
[34] D. Gogova, P.P. Petrov, M. Buegler, M.R. Wagner, C. Nenstiel, G. Callsen, M. Schmidbauer, R. Kucharski, M. Zajac, R. Dwilinski, M.R. Phillips, A. Hoffmann, R. Fornari, Structural and optical investigation of non-polar (1100) GaN grown by the ammonothermal method, J. Appl. Phys. 113 (2013) 203513, , https://doi.org/10.1063/1.4807581.
[35] V. Darakchieva, B. Monemar, On the lattice parameters of GaN, Appl. Phys. Lett. 91 (2007) 031911, , https://doi.org/10.1063/1.2753122.
[36] M. Funato, K. Matsuda, R.G. Banal, R. Ishii, Y. Kawakami, Strong optical polarization in nonpolar (1100) AlxGa1-xN/AlN quantum wells, Phys. Rev. B 87 (2013) 041306(R), https://doi.org/10.1103/PhysRevB.87.041306.
[37] M.B. McLaurin, A. Hirai, E. Young, F. Wu, J.S. Speck, Basal plane stacking-fault related anisotropy in X-ray rocking curve widths of M-Plane GaN, Jpn. J. Appl. Phys. 47 (2008) 5429, https://doi.org/10.1143/JJAP.47.5429.
[38] M.A. Moram, C.F. Johnston, M.J. Kappers, C.J. Humphreys, Investigating stacking faults in nonpolar gallium nitride films using X-ray diffraction, Physica. B: Cond. Matt. 404 (2009) 2189, https://doi.org/10.1016/j.physb.2009.04.010.
[39] M.A. Moram, C.F. Johnston, M.J. Kappers, C.J. Humphreys, Measuring dislocation densities in nonpolar A-plane GaN films, J. Phys. D: Appl. Phys. 43 (2010) 055303, , https://doi.org/10.1088/0022-3727/43/5/055303.
[40] C. Stampfl, C.G. Van de Walle, Energetics and electronic structure of stacking faults in AlN, GaN, and InN, Phys. Rev. B 57 (2008) R15052, https://doi.org/10.1103/PhysRevB.57.R1505.
[41] U. Pietsch, V. Holy, T. Baumbach, High-Resolution X-Ray Scattering: From Thin Films to Lateral Nanostructures, second ed., Springer-Verlag, New York, 2004.
[42] S. Mita, R. Collazo, A. Rice, J. Tweedie, J. Xie, R. Dalmau, Z. Sitar, Impact of gallium supersaturation on the growth of N-polar GaN, Phys. Status Solidi C 8 (2011) 2078, https://doi.org/10.1002/pssc.201001063.
[43] I. Bryan, Z. Bryan, S. Mita, A. Rice, J. Tweedie, R. Collazo, Z. Sitar, Surface kinetics in AlN growth: a universal model for the control of surface morphology in III-nitrides, J. Cryst. Growth 438 (2016) 81, https://doi.org/10.1016/j.jcrysgro.2015.12.022.